X-ray diffraction from ripple structures on InSb created by femtosecond laser pulses

Jurgilaitis, Andrius

2008

X-ray diffraction from ripple structures on InSb created by femtosecond laser pulses

MAXLAS report by
Andrius Jurgilaitis

Lunds Reports on Atomic Physics, LRAP-397
Lund, August 2008

Contents

Introduction

The research project presented in this report is about the investigation and characterization of laser induced surface structure on asymmetrically cut InSb crystal. Experimental and theoretical work was performed during my research studies at MAX-lab and Lund University. It addresses the possibility of using non-thermal melting in repetition mode as timing diagnostic for short pulse X-ray sources.

This work can be seen in the context of ultrafast X-ray science, which is an advancing field in today's science. Technological advances in laser and synchrotron radiation technique provide the opportunity to study ultrafast phenomena such as phase transitions, electron-phonon interaction, non-thermal melting or chemical reactions. Pump-probe techniques are a versatile tool for such experiments. Time resolved measurements can be used to make molecular movies of molecular motion. Future brilliant light sources such as free electron lasers (FEL) will allow to do such experiments with femtosecond temporal resolution.

The main technique in this work was X-ray diffraction, which is a powerful tool to probe crystal structure. Experiments were carried out at MAX-lab in Lund at beamline D611.

Laser – induced surface structures

When a laser beam interacts with matter a series of complex events are triggered. A material can be excited, molten, and loose it's original structure due to the energy transfer. Laser excitation can bring the solid to a state far from equilibrium. Laser matter interaction has been studied since the 1960's, when the first laser was invented. An interesting surface behavior was observed by M. Birnbaum[1] when the laser fluence was close to the melting threshold of the material. Spontaneous, highly periodic, permanent surface structures or "ripples" can be created on the surface of a solid material irradiated with pulsed or CW light by a single or multiple laser shots.
Mostly, ripples run perpendicularly to the incident electric field. At normal incidence the ripple spacing is close or equal to the excitation light wavelength. It was found that ripples occur preferentially with three different periodic spacings given by:

$$\Lambda_{\pm} = \lambda/(1 \pm \sin\theta) \text{ and } \Lambda_{C} = \lambda/\cos\theta, \qquad (1)$$

where θ is the laser angle of incidence with respect to the surface and λ the wavelength of the laser radiation. Emmony et al.[2] first suggested an explanation, where interference of an incident wave with the scattered wave from imperfections such as dust particles or scratches will produce the intensity modulation. As a consequence of this intensity modulation, the melting threshold was periodically exceeded. Possible ripple formation from the liquid phase was proposed by N.C. Kerr et al[3]. which is schematically shown in Fig. 1.

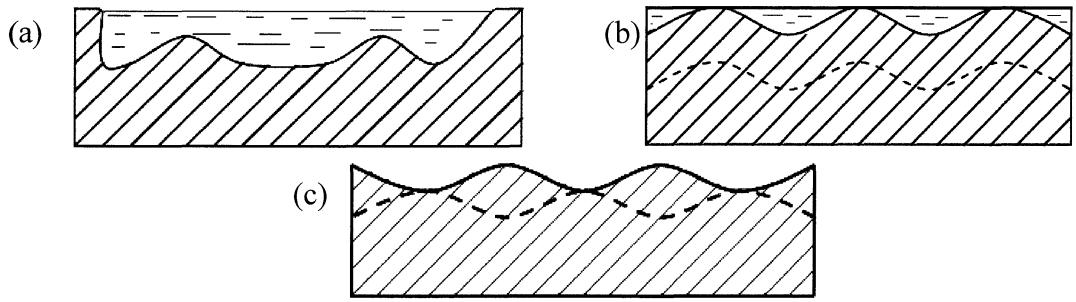

Fig. 1: Plausible ripple formation mechanism for a liquid surface. Where (a) shows fully molten surface on top of the crystal, (b) some points just solidified and pin remaining molten material, (c) formed surface ripples.

If the material is irradiated with an average fluences well above the melting threshold the surface melts completely but some parts will be subjected to higher fluences and melt deeper than others. Since transverse energy transport is slow, the solid / liquid interface maps the inhomogeneous energy deposition due to the interference effect and retains the sinus-like contour. During the resolidification process the sinus-like contour grows until it reaches the surface. Cooling of the molten material can be calculated by solving the thermal conduction equation. As soon as resolidified material reaches the surface it becomes locked to it i.e. it can not grow any further. At this point liquid and solid matter are separated (Fig. 1 (b)). The locked parts stay and after resolidification they form the valleys between ripples provided that the density of the molten phase is higher than that of the solid. The areas between these parts rise up and form the final rippled surface.
At a first glance the study of such surface behavior seems to be rather academic, but in fact it has some direct applications. For example it is the best candidate for diamond micromachining and designing due to its precision and ablation free processing.[4] Furthermore the rippled surface can work as a grating and disperse light. Such effect was recently used by Vorobyev et. al. where they managed to change highly reflective metal into a highly absorptive[5] one, a so called black metal.

Instabilities in crystals

Crystal instabilities destroy "ideal" crystal structure and introduce defects in the crystal. Instabilities generally appear at the place where the dynamics is fastest (the surface), that is where formation of bumps or holes starts. There are four classes in which growth instabilities can by divided: (a) diffusion instabilities (appears when the crystal is growing from the dense phase, as a result of it dendrites[♣] are formed); (b) kinetic instabilities (appears when the growth process is not optimal and does not fulfill anymore the minimum energy principle); (c) thermodynamic instabilities (appears during growth of one material on top of another); (d) geometric instabilities[6]. InSb is a high atomic number solid, which has two different components In and Sb.

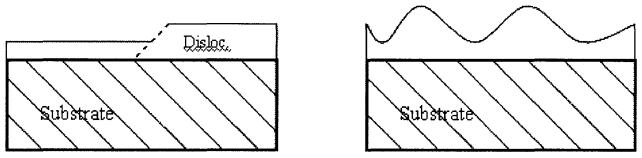

(a) (b)

Fig. 2: Energy minimization possibilities; (a) creation of misfit dislocation, (b) creation of waves at the surface

It is hard to predict how a crystal will minimize energy during relaxation, whether a misfit dislocation is created or a 3D modulation of the surface. Kinetic factors are very important in crystal / superlattice growth and play a dominant role in surface morphology.[7] Unfortunately this kind of instability is not understood very well yet.

Surface relaxation and reconstruction. It can be easily seen that on a surface, due to the absence of neighboring atoms on one side, the interatomic forces in the uppermost lattice planes are considerably changed. The equilibrium conditions for surface atoms are modified with respect to the bulk, so the surface atomic structure usually does not agree with that of the bulk.

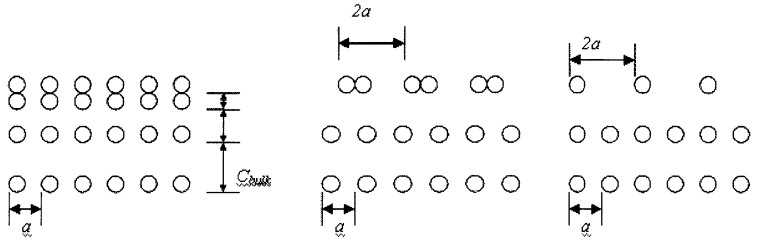

(a) (b) (c)

Fig. 3: Schematic side view of the characteristic rearrangements of surface atoms of cubic lattice constant *a*. (a) relaxation of the topmost atomic layer normal to surface (different lattice spacing); (b) reconstruction or the topmost atomic layer into a surface with double periodicity distance; (c) missing row reconstruction with missing atoms in the topmost lattice plane.

Figure 3 schematically shows some characteristic rearrangements of surface atoms.[8] Figure 3a shows pure compression (or extension) of the topmost atomic layer. In this case, the 2D lattice, i.e. the periodicity parallel to the surface within the topmost atomic layer is the same as for the bulk. In Fig. 3b shifts parallel to the surface can change the periodicity parallel to the surface. The 2D unit cell has dimensions different from those of a projected bulk unit cell. Reconstructions also include surface

♣ dendrite is a crystal that develops with a typical multi-branching tree-like form.

atomic configurations in which atoms or a whole row of atoms are missing in comparison with the bulk. In Fig. 3c the surface periodicity is always different from that of the bulk.

Pump-probe technique

There is a vast number of phenomena in nature which take place in a very short time (picoseconds or femtoseconds). Such processes are for example chemical reactions, electron-phonon scattering, or photo dissociation.
So called pump-probe techniques can be used to resolve fast phenomena if short pulses are available. The idea behind it is to initiate a structural change (pump) which is subsequently examined after a set delay (probe). By varying the delay between pump and probe the structural change is measured as a function of time. In order to observe ultrafast processes, short pulses must be used. To make two synchronized trains of pulses the laser beam must be split into two different arms. In order to set the delay between pump and probe a delay stage is usually used controlling the delay by the difference between optical paths. Figure 4 shows a typical pump probe scheme.
There are several variants of the pump-probe technique depending on what kind of pulses is used. Optical pump-probe, optical pump / X-ray probe or X-ray pump-probe. Depending on the phenomenon monochromatic or white light can be used. To observe structural dynamics in matter visible pump X-ray diffraction probe is the most promising technique. Light excitation induces intensity variations of the Bragg reflections and changes in peak position. The peak shifts are related to changes in lattice dimensions (variation of lattice constant). Laser excitation can change the lattice constant via thermal expansion, electronic strain and / or the generation of acoustic waves. Acoustic waves in the crystal propagate with the speed of sound. It was shown that it is possible to observe laser excited acoustic phonons in InSb. Frequencies of the oscillations as a function of deviation from the Bragg angle were measured and successfully modeled in an earlier study.[9] Other important fields where the optical pump X-ray probe technique turned out to be very useful is the study of the motion of charges in a terahertz light field[10] or the study of the ultrafast solid to liquid phase transition which occurs at the surface of semiconductors which are exposed to intense laser irradiation. Typically a layer of a few tens of nanometers will melt in a few hundred femtoseconds.[11]
In case of the optical pump / X-ray probe technique one needs to address the fact that optical light and X-ray light have different cross sections. The cross section for X-ray photons (about 10^{-15} cm^2) is usually smaller than the cross section for optical photons (about 10^{-13} cm^2).[12] In the case of semiconductors this simply means that optical photons penetrate only few hundreds of nanometers into the material while X-ray probe (1-2 Å) usually several micrometers. To overcome this situation asymmetric reflections can be used.

To record fast processes a streak camera can be used. Such cameras are able to measure the temporal behavior of optical events on a very short time-scale. Beamline D611 is equipped with a picosecond resolution streak camera. It provides ultimate sensitivity down to the single-photon level. The working principle of a streak camera is shown in Fig. 5. Incoming X-rays strike a photocathode, the generated photo electrons travel towards an accelerating mesh and get accelerated. The accelerated photoelectron bunch passes through a pair of sweep plates. The sweep plates are driven by a fast ramped voltage provided by a photoconductive switch, which is triggered by the laser pulse. Another part of the laser beam is directed towards the photoelectrode of the camera and serves as temporal reference. The swept photoelectron bunch transforms the temporal dimension into a spatial dimension. To match the speed of the charge on the sweep plates to that of the photoelectrons the conductive path on the sweep plates has meander shape. Finally the photo electrons are focused by a magnetic lens onto a phosphor screen

which is subsequently imaged onto a CCD chip. The temporal information can be calculated from the spatial position on the screen.

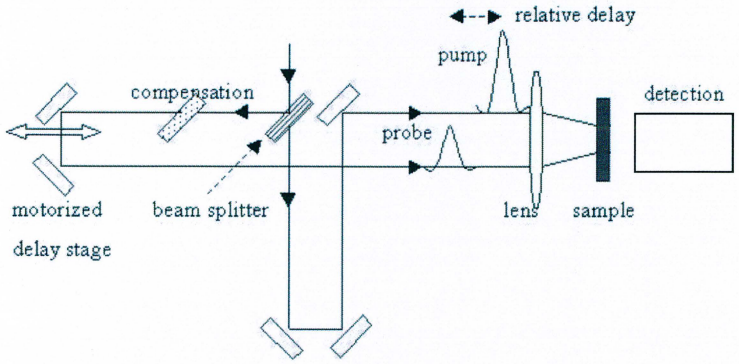

Fig. 4: Scheme for pump probe technique.

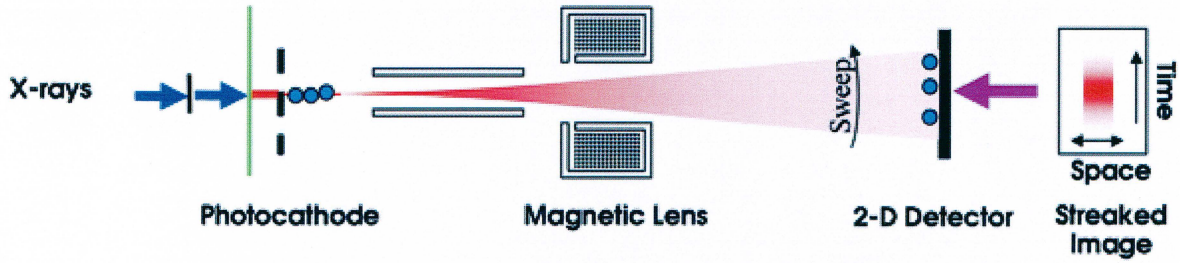

Fig. 5: The principle of a streak camera.[13]

InSb and asymmetric reflections

Indium antimonide (InSb) is a narrow band gap (0.17eV at 300K) III-V group semiconductor material. Such crystals are widely used as infrared detectors, since it is very sensitive in the 1 – 5 μm wavelength region.[14] It has zinc blende (FCC) structure and consists of two heavy elements with Z = 49 and Z = 51 for indium and antimony respectively. Hence it is a suitable material for laser pump / X-ray diffraction probe experiments due to its high X-ray scattering power.

A suitable way to enhance the diffracted X-ray signal is to modify the diffraction geometry by changing the crystal cut angle. We were using an asymmetrically cut InSb (111) crystal where the angle between surface and lattice planes was about 17°. Information about the surface layer is always hidden by the large signal from deeper lying parts. The X-ray absorption depth for Bragg reflections usually lies within 1 – 10 μm. The scattering signal comes from all of the layer simultaneously.[15, 16] In perfect or near perfect crystals penetration depth of the X-rays is determined almost entirely by extinction.[17] There are two ways to decrease the penetration depth. One can use softer X-rays or asymmetric reflections. X-rays coming at grazing incidence geometry yield a wide rocking curve due to the reduced penetration depth.[18] In Fig. 6 three cases of diffraction from perfect crystals with different asymmetries is presented. The Bragg peak changes its shape, amplitude and position depending on what experimental geometry is used.

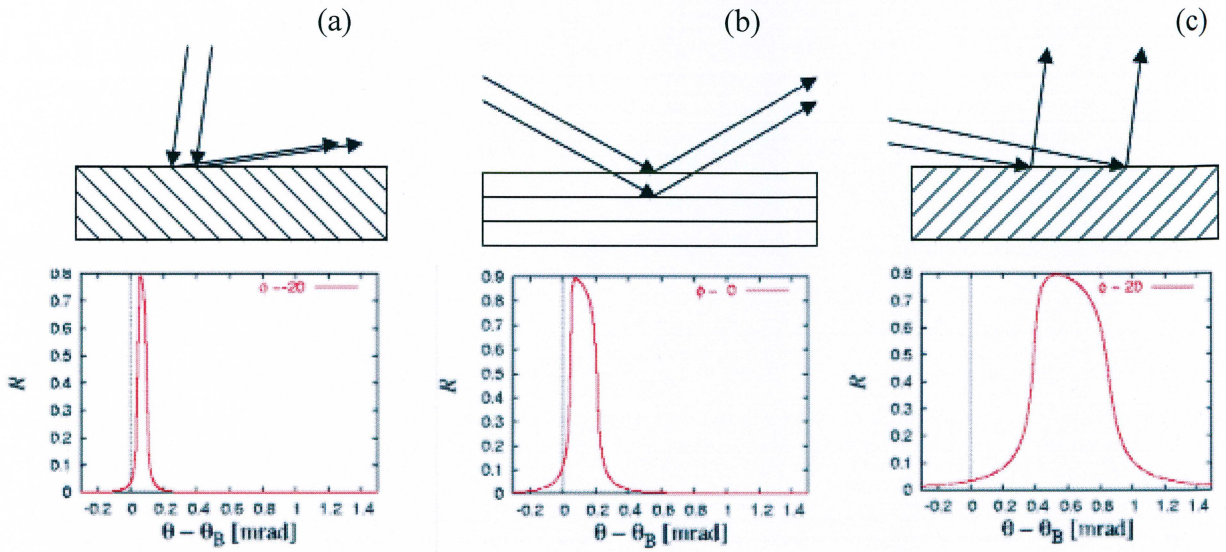

Fig. 6: Bragg reflection occurring from a sample (a) with positive asymmetry, (b) symmetrically and (c) with negative asymmetry. For each asymmetry case calculated rocking curves are presented[19].

The asymmetry of the calculated rocking curves comes from X-ray absorption in the material. From Fig. 6 it is clear that an asymmetric reflection is a simple method for reducing the penetration depth and probing the crystal near the surface. By understanding how certain structural changes affect the rocking curve shape it is possible to solve the inverse problem i.e. to identify structural changes from the shape of the rocking curve. In a section below, X-ray reflectivity simulations are described in more detail, where specular reflection, absorption in amorphous layers and asymmetry factors are taken into account.

X–Ray diffraction

X-rays were discovered by Röntgen in 1895. He observed phenomena which looked very much like diffraction[19], but were not understood at that time. Diffraction occurs when electromagnetic radiation interacts with a periodic structure where the periodicity is about the same as the wavelength of the radiation. If the wavelength and the inter-atomic distances are roughly the same, diffraction patterns, which reveal the repeating atomic structure, are formed. In 1912, Max von Laue recognized that X-rays would be scattered by atoms in a crystalline solid if there is a similarity in spatial scales. X-rays have wavelengths on the order of angstroms (typical interatomic distances in crystalline solids). X-ray photons and electrons are scattered by the electron shells in contrast to neutrons which are scattered by the nuclei. To study atomic structures X-rays are the best candidate.
Diffraction from a three dimensional periodic structure such as atoms in a crystal is called Bragg diffraction. Bragg diffraction is a consequence of interference between waves reflecting from different crystal planes. The condition of constructive interference is given by expression below:

$$2d\sin\theta = n\lambda, \qquad (2)$$

where θ is the angle of the diffracted wave, λ the wavelength of the X-rays, d the distance between lattice planes, and n the diffraction order.

Each atomic plane reflects a very small fraction of the incident amplitude. For some angles of incidence (Bragg angle) the waves reflected from neighboring planes will show a phase difference that leads to constructive interference. From equation (2) it is clear that the greater the wavelength the larger the Bragg angle if the lattice constant is kept constant or the larger the lattice spacing the smaller is the Bragg angle for a given wavelength.

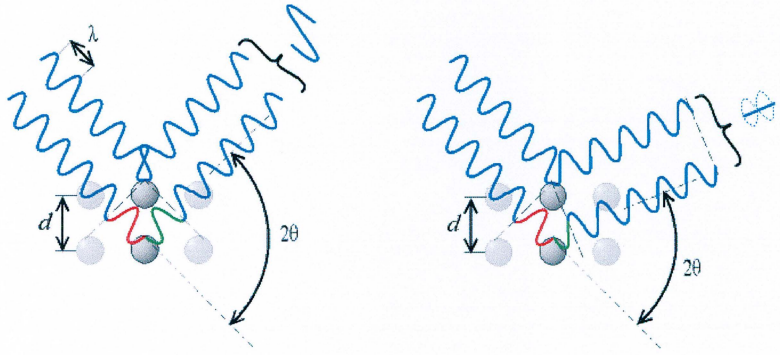

Fig. 7: The phase shift causes constructive (left) or destructive (right) interferences[20].

Atomic force microscope

The atomic force microscope is a powerful tool for studies of nanoscale structures on both conducting and insulating surfaces. A small atomically sharp tip at the end of a cantilever is brought close to a surface with the use of piezo elements and starts scanning the surface. Tips are typically made from Si_3N_4 or Si, extending down from the end of a cantilever. If the tip touches the surface the cantilever bends, which is measured by a laser beam. Therefore a diode laser is focused on to the back of the reflective cantilever (Fig. 8). While the sharp tip scans the surface, a feedback system tries to keep either the laser signal constant (to obtain height information), or the height above the sample surface (to obtain force information). The cantilever scans the surface, moving up and down, following the contours of the surface. The topology will be displayed on a computer monitor. The scanning in the *x, y* direction and the feedback compensator in *z* direction is controlled by a very sensitive piezo tube. The tip senses the force when it approaches the surface of the sample. The force can be derived from the Lennard-Jones potential. It is composed of two parts: (a) a long range attractive force (Van der Waals force) and (b) a short range repulsive force arising from the Pauli exclusion principle. The Lennard-Jones potential is not linear, so AFM can work in several modes using certain regions of this curve.

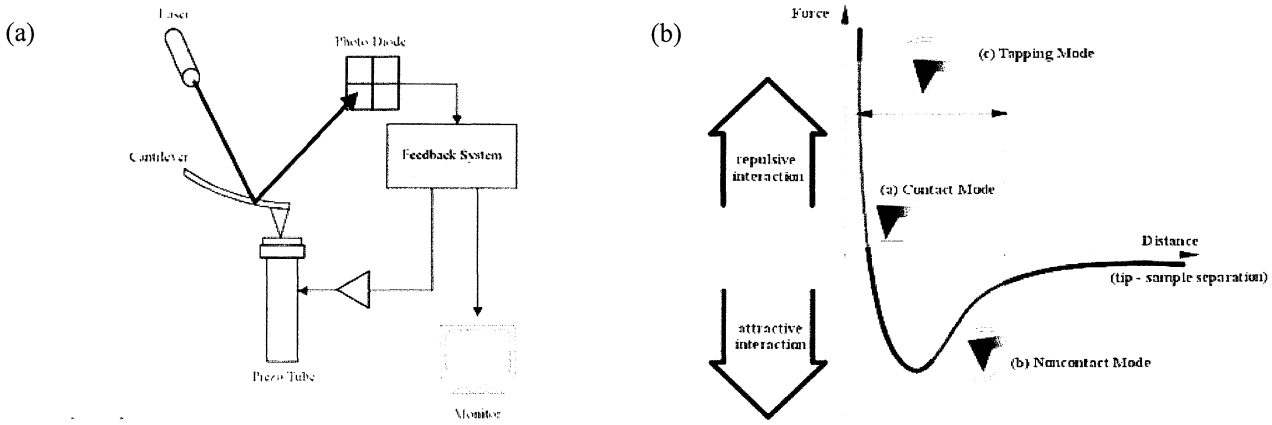

Fig. 8: (a) Schematic AFM structure (b) Potential between tip and sample

Non-contact mode. In this mode the cantilever is set to vibrate at its resonance frequency at a few nanometers (5-15 nm) above the sample surface. Attractive Van der Waals forces are acting between the tip and surface. When the tip senses the surface the vibration is damped and the feedback retracts the tip a little until the resonance frequency is restored.

Contact mode. In this mode the tip is in physical contact with the sample surface all the time while scanning. The force on the tip is repulsive with a mean value of 10^{-9} N. In contact mode AFM the deflection of the cantilever is sensed and compared in a DC feedback amplifier to a set value of deflection. If the measured deflection is different from this set value the feedback amplifier applies a voltage to the piezo to raise or lower the sample relative to the cantilever to restore the set value of deflection. The tip actually hits the particles and structures, so this mode offers a high lateral resolution, but there is large risk to damage the sample.

Tapping mode. Tapping mode is a compromise between the two earlier described modes. This mode allows getting high resolution topographic imaging of the sample surfaces and the risk to damage the sample is quite small. Tapping mode imaging is implemented in ambient air by oscillating the cantilever assembly at or near the cantilever's resonant frequency using a piezoelectric crystal. During tapping mode operation, the cantilever oscillation amplitude is maintained constant by a feedback loop. The digital feedback loop then adjusts the tip-sample separation to maintain constant amplitude and force on the sample.

Experiment

I. *Experimental setup.* The experiment was carried out at beamline D611 at the MAX II electron storage ring. MAX II is a 3rd generation synchrotron source with 1.5 GeV electron energy and 90 m circumference operational since 1996. Figure 9 shows a schematic of the D611 beamline, which is dedicated to laser-pump X-ray probe experiments. X-rays are generated in a bending magnet and later focused by a gold coated toroidal mirror. The beamline has a double crystal monochromator equipped with Si(111) crystals and multilayer mirrors, where the X-ray energy can be selected in a range between 2.5 and 8 keV. A 400×200 μm^2 beam size can be reached with 7×0.7 $mrad^2$ divergence (horizontal × vertical).

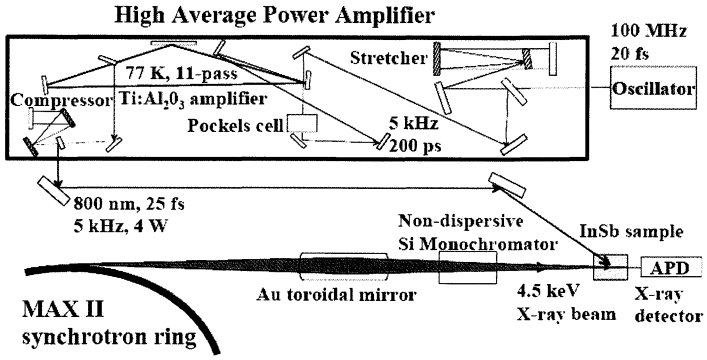

Fig. 9: Sketch of beamline D611 at MAX-lab.

The beamline is equipped with a laser system consisting of a passively modelocked Ti:sapphire oscillator followed by a cryogenically cooled Ti:sapphire multipass laser amplifier. It operates with up to 10 kHz repetition rate at an average power up to 7 W. The wavelength is centered around 780 nm, and the pulse duration is about 70 fs. The oscillator runs at 100 MHz repetition rate and can be locked to the radiofrequency signal from the accelerating cavities of the synchrotron ring with a jitter below 10 ps. Laser light with fluences up to 100 mJ/cm^2 were used to excite the InSb sample, which was mounted on a sample holder, with five degrees of motional freedom. X-rays impinged on to the sample with 0.8° angle of incidence with respect to the surface. This reduced the X-ray penetration depth mainly due to absorption and hence makes the probe more sensitive to structural changes near the surface. In this experiment the laser and electron storage ring were running asynchronously, because temporal resolution was not required. The intention was to measure the accumulated damage post mortem. The diffracted signal from the sample was collected with an avalanche photo diode. Rocking curves from different parts on the sample were recorded.

II. *Experimental details.* The attenuation lengths in matter for X-rays and visible light are different. At gracing incidence X-rays penetrate a surface layer of only few tens of nanometers thickness while at steep incidence they reach a depth of a few micrometers. To make sure that the probe depth matches the thickness of the laser irradiated surface layer the X-rays must come at a grazing incidence. We set the X-ray energy to 5.12 keV and 0.8° angle of incidence with respect to the surface. The experimental sample geometry is presented in Fig. 10. An asymmetrically cut (−17°) InSb crystal was used. The InSb wafer was placed in the vacuum chamber and exposed to femtosecond laser pulses with the following fluences and incident angles with respect to the surface: 10, 20, 30, 40, 50, 60, 80, 100 mJ/cm^2 and 5°, 10°, 15°, 20°, 25°, 30°, 35°, 40°.

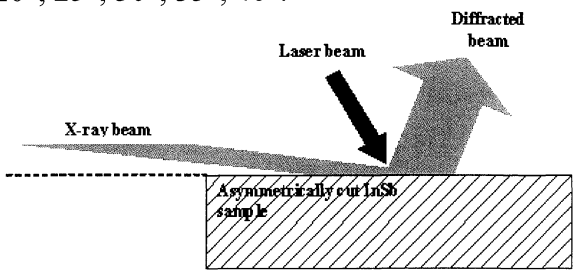

Fig. 10: Experimental geometry.

The laser beam was *p*-polarized irradiating a surface area of 4×0.4 mm^2, which is considerably larger than the X-ray beam profile. To monitor the beam profiles a thin phosphor layer for the X-rays and a paper with millimeter scale for the laser were placed on the sample surface. Micrometer resolution

stepper motors were used to provide 0.5 mm spacing between the laser irradiated strips sideways and 1 mm between consecutive rows of strips.

In order to compensate for the variation of laser footprint on the InSb sample with incident angle, different exposure times for different laser incidence angles were used in order to keep the total accumulated fluence constant. Table 1 gives details of this experiment and Table 2 shows the calculated periodicities of the ripple structure that can be expected.

Table 1 Laser beam and experiment details.

Laser irradiation angle φ (deg)	Beam size horizontal/vertical (mm)		Exposure time (s)
5	0.426	1.8	22
10	0.443	0.94	42
15	0.426	0.59	68
20	0.459	0.412	97
25	0.443	0.254	157
30	0.443	0.275	145
35	0.459	0.278	145
40	0.443	0.228	175

To avoid contaminants such as water vapor and carbon droplets the sample was kept under vacuum all the time between laser exposure and X-ray examination. X-ray diffraction from the irradiated sample areas was performed at grazing incidence. The X-ray reflectivity was measured in an energy interval 5.1 – 5.3 keV while the diffraction angle was kept constant.

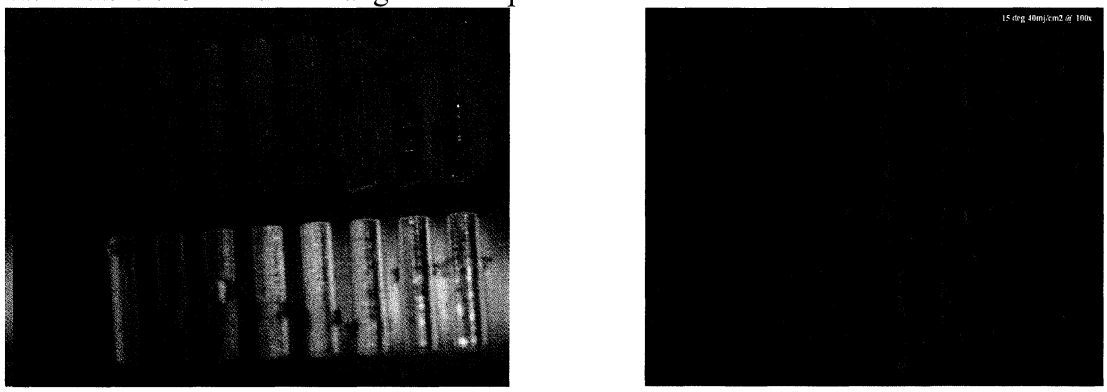

Fig. 11: (a) InSb sample surface after laser irradiation. The top set of strips was irradiated with laser incidence angle of 20° the bottom with 40°. (b) OM image of laser induced surface structure at 40 mJ/cm^2 and 15° laser incident angle.

III. *Experimental results and interpretation.* Laser induced surface structures on the InSb sample were studied with: optical microscope (OM), atomic force microscope (AFM), scanning electron microscope (SEM), energy dispersive X-ray spectroscopy (EDS) and X-ray diffraction. The obtained ripple structures seen in the OM picture qualitatively agree with the ripple formation model given by Young et al[21].

Table 2 Calculated ripple periodicities from the (1) notation.

φ (deg)	Θ (deg)	Λ_+ (m)	Λ_- (m)	Λ_C (m)
5	85	3.91 e-7	2.04 e-4	8.94 e-6
10	80	3.92 e-7	5.13 e-5	4.49 e-6
15	75	3.96 e-7	2.28 e-5	3.01 e-6
20	70	4.02 e-7	1.29 e-5	2.28 e-6
25	65	4.09 e-7	8.32 e-6	1.84 e-6

30	60	4.18 e-7	5.82 e-6	1.56 e-6
35	55	4.28 e-7	4.31 e-6	1.35 e-6
40	50	4.41 e-7	3.33 e-6	1.21 e-6

Early works on rippled surface structures are based on the model suggested by Young et al., which explains ripple formation by interference effects. The theory works well with CW but not so well with pulsed lasers. The first laser pulse causes random roughening, while the subsequent pulses create periodic ripples (S+, S− and c fringes)[22]. The wavelength, polarization and incident angle of the laser radiation determine the spatial period. The S+ and S− ripples occur perpendicularly to the polarization and have a period given by $\Lambda_{\pm} = \lambda/(1 \pm \sin\theta)$. S− is usually dominant[23]. The c type of fringes are rarely formed and run parallel to the polarization, and the period is given by $\Lambda_C = \lambda/\cos\theta$. All types of ripples described in the literature were found on the InSb sample. Ripples start to grow well with irradiation fluences above 20 mJ/cm^2 and laser angle of incidence above 5° with respect to the sample surface. Figure 12 shows images of these structures from InSb irradiated with different fluences at 15° laser incidence angle. It is possible to observe different ripples with periodicities 1.2 – 5 μm. At low fluences, ripples run parallel to the incident electric field. At higher fluences short period ripples are overgrown by large spatial periodicity structures. Such surface behavior was observed in all samples at all laser incidence angles. Equation (1) does not work well for femtosecond laser pulses. The spacing of the ripples formed by femtosecond pulses is not influenced by the incidence angle of the laser beam[24]. The fluence of the laser beam profile influences the depth but not the spacing. Nevertheless a fair agreement with classical ripple formation model was found. At 25° laser incident angles ripple periodicities were close to the result given by equation (1).

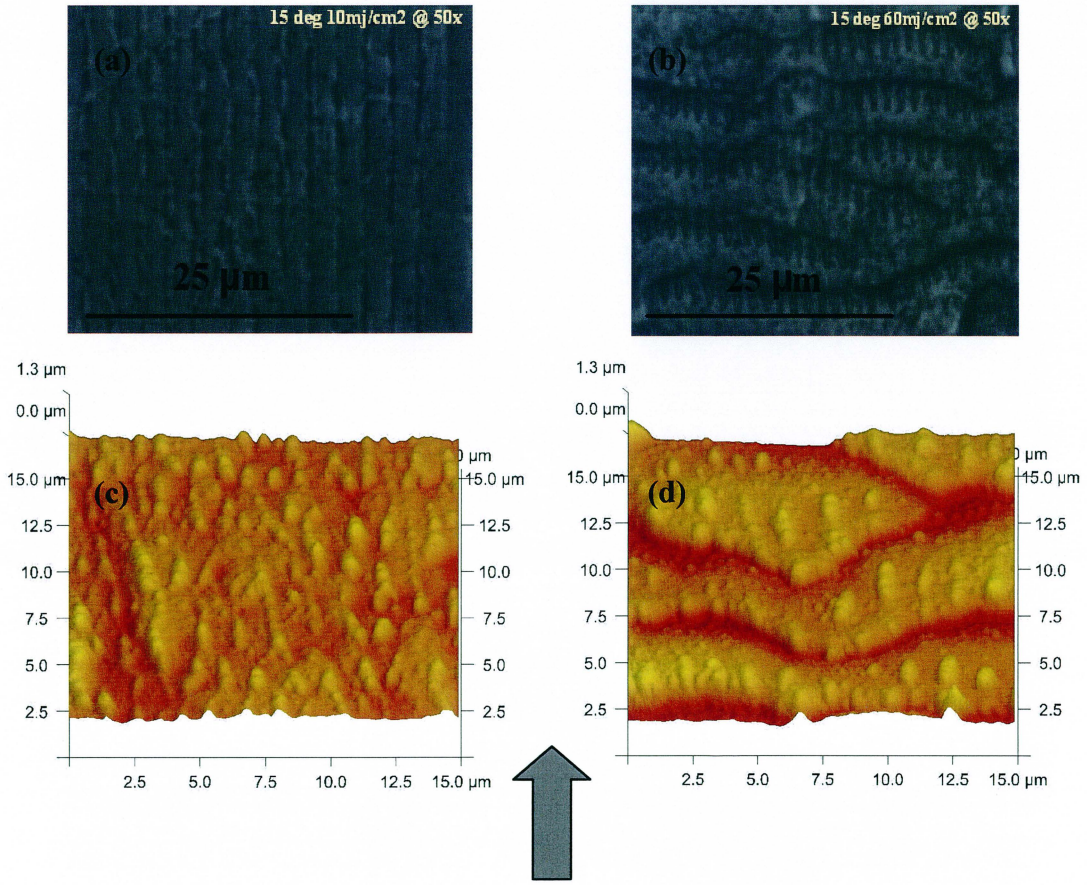

Fig. 12: OM and AFM images of laser irradiated surface structure at 15° laser incidence angle and a fluence of (a) 10 mJ/cm^2, (b) 60 mJ/cm^2, (c) 30 mJ/cm^2 and (d) 50 mJ/cm^2. The arrow indicates the direction of laser incidence.

It was found that the ripple structures do not depend on surface orientation and follow only the laser irradiation direction. This is in agreement with other experiments[25, 26, 27, 28] which above that found that the ripple structure is independent of the atmosphere, and that ripples appear most pronounced at fluences close to the melting threshold.
Since the formed surface structures have different height and different periodicities a combination of various inspection tools is needed. Optical, atomic force and scanning electron microscopes were used to extract surface properties such as periodicity, ripple height, and surface roughness.

Observed variations of the surface structures suggest that the crystal structure varies, which can influence X-ray diffraction (shape of the rocking curve). For laser fluences above the melting threshold the laser melts a thin surface layer on the sample. Non-thermal melting occurs if the laser fluence is high enough[29]. In case of InSb this is about 30 mJ/cm^2 and above. In principle the molten InSb can resolidify to a crystal or just freeze in amorphous phase. Post mortem X-ray diffraction measurements of laser irradiated areas showed higher reflectivity values if the laser fluence comes close to the melting threshold an effect known as laser annealing. If the laser fluence lies well above the melting threshold, in the case of InSb between 25 to 40 mJ/cm^2 depending on angle of laser incidence, reflectivity goes down permanently, i.e. even after the laser is switched off. For very high per pulse laser fluences and sufficient long exposure times the crystal structure is destroyed entirely and the diffracted beam disappears. A study[30] showed that under suitable conditions the molten InSb can regrow to a "perfect" crystal after femtosecond laser irradiation. The same conclusion can be drawn from the outcomes of the present study. The recorded X-ray reflectivity from the "fresh" sample was lower than the reflectivity after laser irradiation with fluences up to about 25 to 40 mJ/cm^2 depending on angle of incidence. It can be explained by an initially poor surface quality (surface scratches, contaminants) in combination with a small X-ray penetration depth at grazing incidence. After laser irradiation the InSb crystal regrows in better order. By increasing the laser fluence up to 40 mJ/cm^2, the reflectivity increases too. For fluences above 40 mJ/cm^2 the reflectivity goes down again. This decrease in reflectivity can be due to a growing number of imperfections built in during crystal regrowth[31]. For fluences above 80 mJ/cm^2 the X-ray reflectivity disappears due to a thick amorphous layer on the surface.

IV. *Rocking curve simulation.* In the X-ray diffraction measurements we find asymmetric rocking curves on surface areas with rippled surface structures. Figure 14 shows some measured rocking curves after laser irradiation at 10° and 20° incidence angle,

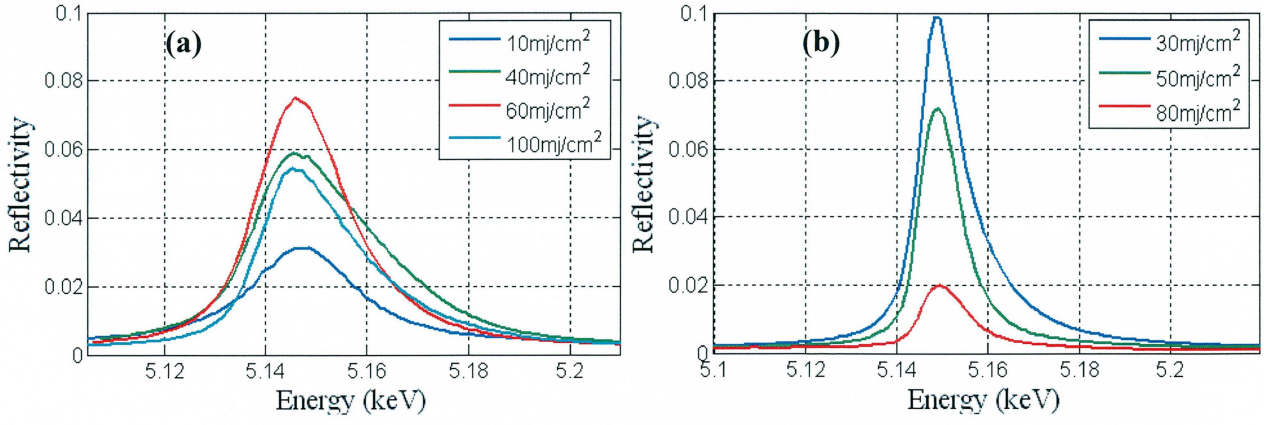

Fig. 13: Experimental rocking curves at 10° (a) and 20° (b) laser incidence angle.

In order to understand the observed asymmetric rocking curves, X-ray diffraction simulations were carried out. Effects from strain, specular X-ray reflection, X-ray absorption in amorphous layer, ripple height and ripple periodicity were taken into account. To calculate diffraction from strained crystals the

GID_SL code from S. Stepanov's X-ray server was used.[32] Rocking curves with strain up to 10 % were calculated and are shown in Fig. 14. These calculations were done for 5.12 keV X-ray energy and –17° angle of asymmetry, i.e. the angle of Bragg planes with respect to the surface. The expansive strain moves the diffraction peak to the low energy side. From Bragg's law it is immediately clear that in order to diffract from a lattice with an increased lattice constant a longer wavelength is required to fulfill the Bragg condition. The simulations suggest that at least homogeneous strain does not influence the shape of the measured rocking curve. Inhomogeneous strain, i.e. strain with a non-vanishing gradient in principle could alter the shape. Though, the probed surface layer is so thin 30 nm that the strain gradient would have to be extreme to have a measurable effect.

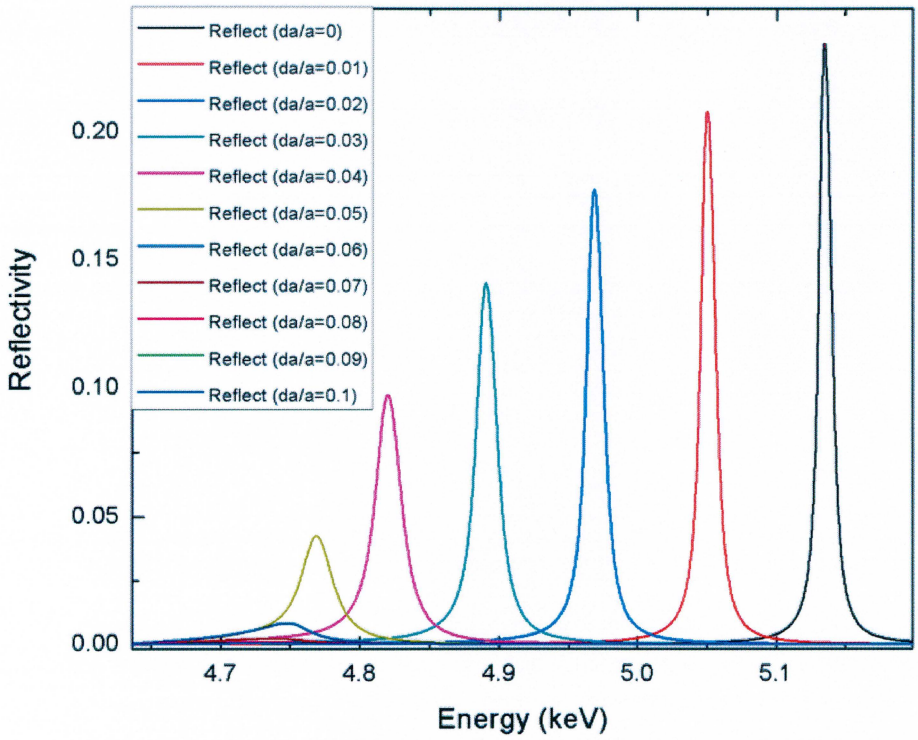

Fig. 14: Rocking curves with induced strain in the lattice.

In order to simulate the effects of the laser induced rippled structure X-ray reflectivity was simulated from an InSb crystal with a perfectly sinusoidal surface. The sinusoidal surface periodicity and amplitude were directly taken from AFM measurements. A schematic of the simulation geometry is presented in Fig. 15. The simulation was done with 8.5 μm ripple periodicity and 1.7 μm ripple height.

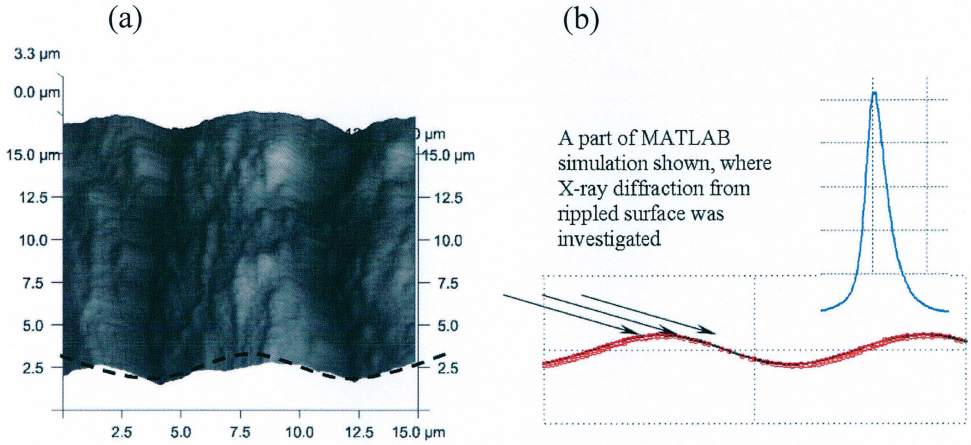

Fig. 15: (a) AFM image of rippled surface structure, surface was irradiated with 50 mJ/cm^2 at 25° laser incidence angle. Measured ripple properties (periodicity and height) were used in the simulation. (b) Grazing incidence X-ray irradiation of rippled surface which turns out to be the origin of the rocking curve asymmetry.

For the simulations a MATLAB code has been developed. It does the calculation in three steps. First the rippled surface structure and the laser incidence are simulated using experimentally measured values. In a second step the local variations of the angle of asymmetry[♣] are calculated and saved. This step shows that the local asymmetry angle varies between 0° and 2° depending on the laser incidence angle. On the basis of these parameters rocking curves are simulated for different asymmetry angles (17°–18.6°). This was done using the ***GID_SL*** code.[12] Figure 16 shows the evolution of the rocking curve as the angle of asymmetry changes. The reflection peak moves to higher energies and goes down in amplitude due to X-ray absorption. Above that a broadening of the curve is observed which is directly related to the X-ray penetration depth. The smaller the penetration depth i.e. the thinner the diffracting layer the broader the diffraction peak. By knowing the distribution of asymmetry angles it is possible to calculate an average rocking curve. A small inset in Fig. 16 shows how in principle the average rocking curve is formed from a set of rocking curves with different angles of asymmetry which helps to understand the shape and the peak shift of the measured rocking curves. The Peak position is directly sensitive to the distribution of asymmetry angles. The model does not yet reproduce absolute reflectivity values. To overcome this discrepancy, several additional factors were taken into account. Specular reflection and X-ray absorption in an amorphous surface layer were included. X-ray absorption and refraction coefficients were taken from online data sources.[33]

♣ Variation in asymmetry angles which comes from the ripple structure due to its sine like shape.

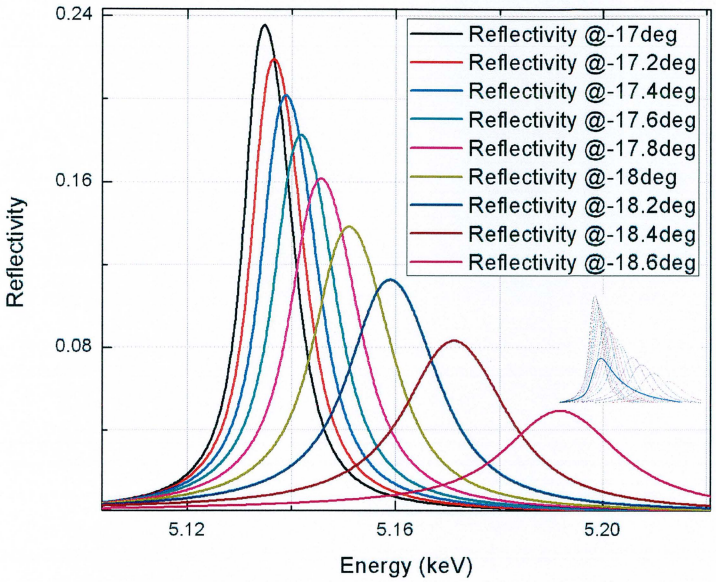

Fig. 16: Simulated rocking curves with varying asymmetry angle. The small inset shows how in principle the average rocking curve is formed from a set of rocking curves with different angles of asymmetry.

The thickness of the amorphous layer is difficult to measure directly. Therefore the inverse problem was solved: the thickness of the amorphous layer was determined that is required to reproduce the measured absolute X-ray reflectivity. Values between 20 and 40 nm were found which is in good agreement with other studies.[9, 12] The results of the simulation are shown in Fig. 17. The simulations suggest that the shape of the rocking curve is determined mainly by asymmetry variations. These variations were estimated from ripple geometry measurements done with AFM and SEM. X-ray reflectivity is reduced mainly due to an amorphous layer on top. At higher laser fluence (>50 mJ/cm^2) the amorphous layer gets thicker and the X-ray reflectivity goes down. Obtained experimental rocking curves were asymmetric and fit well with a simulated weighted-average rocking curve which accounts for asymmetry variations, absorption in an amorphous layer and specular reflection from the surface. The applied physical model gives good agreement with experimental results.

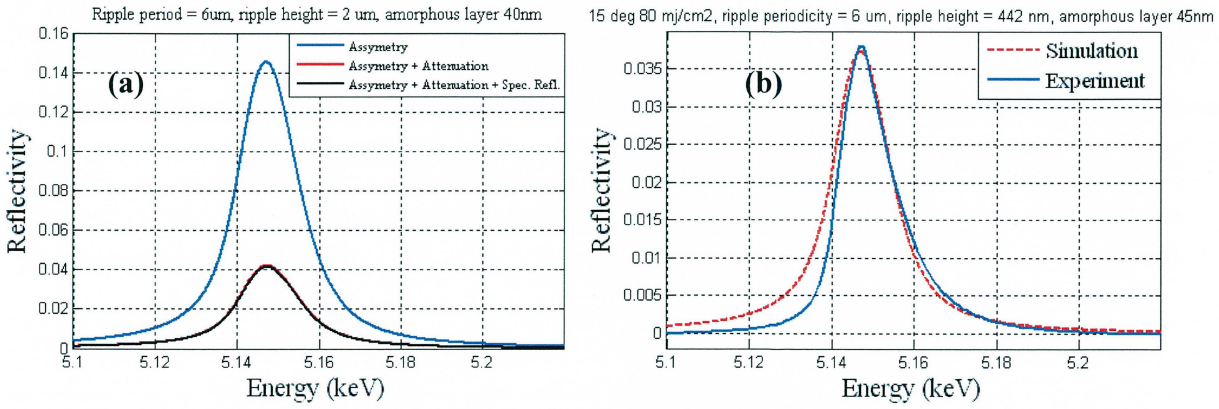

Fig. 17: Simulated rocking curves, where (a) local asymmetry angle variations, absorption in an amorphous layer and specular reflection were taken into account and (b) in comparison to measured rocking curve.

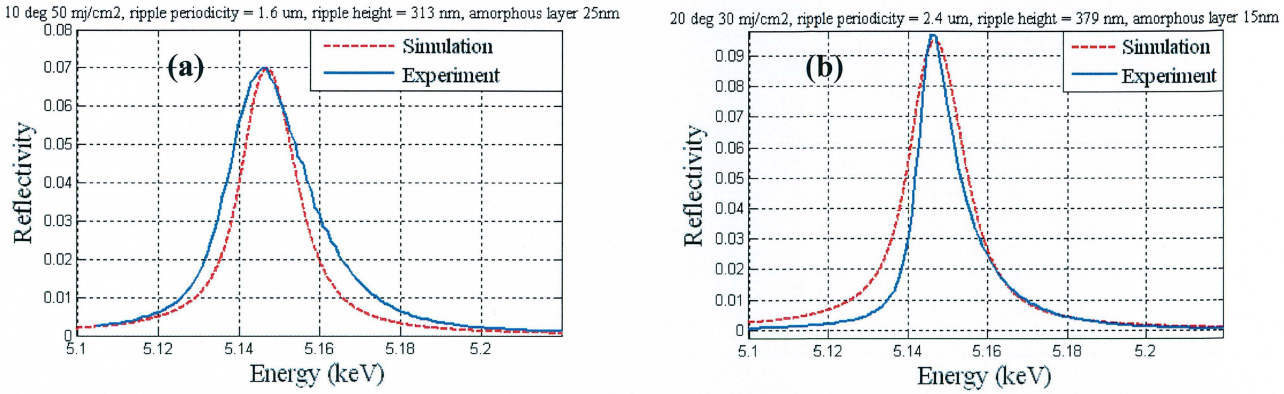

Fig. 18: Simulated and measured rocking curves for (a) 10°, 50 mJ/cm^2 and (b) 20°, 30 mJ/cm^2. In the simulations local asymmetry angle variations, absorption in an amorphous layer and specular reflection were taken into account. Red curve shows simulation while blue is experimentally recorded data.

Conclusions

X-ray diffraction measurements from a sample with laser-induced ripple structures were performed. Surface structures were created by femtosecond laser pulses with different fluences. Ripples were studied with AFM, SEM, OM and X-ray diffraction techniques. Extracted experimental data was directly used to run simulations.

Experiments show that ripples grow best when the laser fluence is close to the melting threshold, i.e. 20 – 30 mJ/cm^2. At higher fluence (>50 mJ/cm^2) an amorphous layer grows and the X-ray reflectivity is reduced. Obtained experimental rocking curves were asymmetric. This effect could be explained with local variations in the angle between surface and incident X-ray beam due to the ripple structure.

X-ray diffraction simulations were performed to understand the measured data. Local variations of the asymmetry factor (comes from rippled surface), amorphous layer on top of ripples (20 – 70 nm), and specular reflection was taken into account. The applied physical model gives good agreement with experimental results.

Acknowledgments

The work presented above could not have been done without the support and the collaboration of many people.

I am thankful to the MAXLAS Marie Curie Early Stage Training Site for a short term position to work in X-ray science and the field of laser physics.

I would like to express my sincere gratitude to my supervisor Professor Jörgen Larsson, who provided a friendly atmosphere during this project. I would like to thank him for admitting me to his research group, for placing trust in me, giving me the opportunity to work in the field of Ultrafast science and for guiding me through.

I would like to thank my co-supervisor Dr. Peter Sondhauss for constant discussions, suggestions and belief in me. I have learned a lot from him.

Many thanks to my colleagues Ralf Nüske, Henrik Enquist and Hengameh Navirian for a lot of useful help, discussions and a nice working environment.

Many thanks to my wife Vilma and my son Kostas for their incessant optimism and love, for being supportive during the time I worked on this research project.

Thanks to everyone who directly or indirectly contributed to the development of this work

Appendix

Early stage training Activity (2007 08 31 – 2008 09 01)

Courses:

Accelerator Technique 7.5 ECTS

Medical Optics 7.5 ECTS

Swedish language course at Komvux

Research tasks:

MAX-lab. Daily work with synchrotron radiation and short laser pulses at a beamline D611 dedicated to the study of ultrafast structural processes. Laser pump X-ray probe technique is used to study ultrafast processes in solid state matter. I was personally responsible for an X-ray diffraction study of rippled structures created with femtosecond laser pulses. I was also involved in time resolved X-ray diffraction studies of non thermal melting of InSb.

Attended summer schools:

Ultrafast X-ray Summer School 2008. Stanford Linear Accelerator Center (USA).

Nordic and European summer school 2008 "VUV and X-ray Research for the Future using FEL´s and Ultra Brilliant Sources"**.** MAX-lab (Sweden).

Research Course on New X-Ray Sciences "New materials in new light". Hamburg (Germany).

References

[1] M. Birnbaum, J. Appl. Phys 36, 3688 (1965).
[2] D. C. Emmony, R. P. Hawson, and L. J. Willis, Appl. Phys. Lett. 23, 598 (1973).
[3] N. C. Kerr, B. A. Omar, S. E. Clark and D.C. Emmony, J. Appl. Phys. 23 884-889, (1990).
[4] Q. Wu, Y. Ma, R. Fang, Y. Liao, and Q. Yu, J. Appl. Phys. Lett. 82, 1703, (2003).
[5] A. Y. Vorobyev and C. Guo, Appl. Phys. Lett. 92, 041914 (2008).
[6] P. Politi, G. Grenet, A. Marty, A. Ponchet, J. Villain, Phys. Rep. 324 271-404, (2000).
[7] N. Kubota and J. W. Mullin, J. Cryst. Growth 152, 203 (1995).
[8] Solid surfaces, interfaces and thin films, fourth edition. Hans Luth, (2001).
[9] J. Larsson, A. Allen, P. H. Buckcbaum, R. W. Falcone, A. Lindenberg, G. Naylor, T. Missalla, D. A. Reis, K. Scheidt, A. Sjogren, P. Sondhauss, M. Wulff, J. S. Wark Appl. Phys. A 75, 467-478 (2002).
[10] A. Cavalleri, S. Wall, C. Simpson, E. Statz, D. W. Ward, K. A. Nelson, M. Rini and R. W. Schoenlein, Nature 442, 664 – 666 (2006).
[11] C. W. Siders, A. Cavalleri, K. Sokolowski-Tinten, Cs. Toth, T. Guo, M. kmmler, M. Horn von Hoegen, K. R. Wilson, D. von der Linde, C. P. J. Barty , science 286, 1340 (1999).
[12] J. Synchrotron Rad. 11, 483 – 489 (2004).
[13] http://www.photonics.com/content/spectra/2007/December/research/89901.aspx
[14] http://www.ioffe.ru/
[15] Nikulin A Yu, Stevenson A W and Hashizume H, Phys. Rev. B 53 8157, (1996).
[16] A. W. Stevenson, Acta Cryst. A49, 174 – 183 (1993).
[17] The theory of X-ray diffraction in crystals, Zachariasen, W. H. (1945).
[18] http://colossus.maxlab.lu.se/tutorials/txrd07/txrd.html, (P.Sondhauss) Ultrafast Science lecture notes 2007.
[19] W. C. Rontgen's Third Communication, (1897).
[20] http://en.wikipedia.org/wiki/Bragg's_law.
[21] J. F. Young, J. S. Preston, H. M. Van Driel, J. E. Sipe, Phys. Rev. B 27, 1424 (1983).
[22] Laser Ablation and desorbtion, edited by J.C. Miller andR. F. Haglund Jr. (Academic, San Diego, CA, 1998), p. 341.
[23] X. C. Wang et al., Applied Surface Science 252 1492 – 1497 (2005).
[24] B. Tan and K. Venkatakrishnan, J. Micromech. Microeng. 16 (2006).
[25] H. J. Leamy, G. A. Rozgonyi, T. T. Sheng, and G. K. Celler, Appl. Phys. Lett. 32, 535 (1978).
[26] G. N. Maracas, G. L. Harris, C. A. Lee, and R. A. McFarlane, Appl. Phys. Lett. 33, 453 (1978).
[27] A. K. Jain, V. N. Kulkarni, D. K. Sood, and J. S. Uppal, J. Appl. Phys. 52, 4882 (1981).
[28] A. Y. Vorobyev, V. S. Makin, and C. Guo, J. Appl. Phys. 101, 034903 (2007).
[29] H. Navirian, H. Enquist, T. N. Hansen, A. Mikkelsen, P. Sondhauss, A. Srivastava, A. A Zakharov and J. Larsson, J. Appl. Phys. 103 (10), (2008).
[30] M. Harbst, T. N. Hansen, C. Caleman, W. K. Fullagar, P. Jonsson, P. Sondhauss, O. Synnergren, J. Larsson, Appl. Phys. A 81, 893 – 900 (2005).
[31] Q. M. Zhang, H. Wang, N. Kim and L.E. Cross, J. Appl. Phys. 75, 454, (1994).
[32] http://sergey.gmca.aps.anl.gov/gid_sl.html.
[33] http://henke.lbl.gov/optical_constants.